Supplementary information

Highly-efficient radiative thermal rectifiers based on near-field gap variations

Bei Yang[a, b], Qing Dai[*a, b]

a. CAS Key Laboratory of Nanophotonic Materials and Devices, CAS Key Laboratory of Standardization and Measurement for Nanotechnology, CAS Center for Excellence in Nanoscience, National Center for Nanoscience and Technology, Beijing 100190, China.

b. Center of Materials Science and Optoelectronics Engineering, University of Chinese Academy of Sciences, Beijing 100049, China.

Corresponding authors: daiq@nanoctr.cn.

Contents

S1. Theoretical description of near-field radiative heat transfer 1

S2. Dielectric properties of materials used in the calculations 4

S3. Comparisons of TRFs under different definitions 5

S4. Effects of graphene's chemical potential and hBN thickness on TRFs 5

S5. Replacing the radiative layers with typical IR polaritonic materials 6

S6. Comparisons of TRFs with previous reports 6

S7. Detailed fitting parameters for $Q = \gamma d^n$ 7

References 8

S1. Theoretical description of near-field radiative heat transfer

For the system illustrated in Fig.1, the reflection coefficient R_n in Eq.2 can be derived from the Fresnel equations for a four-layer heterostructure shown in Fig.S1 via the scattering matrix method[1–3]

$$R_n = \frac{r_n^{12} + R_n^2 e^{2ik_z^n h_1}}{1 - r_n^{12} R_n^2 e^{2ik_z^n h_1}}, \tag{S1}$$

$$R_n^2 = \frac{r_n^{23} + r_n^{34} e^{2ik_z^n h_2}}{1 - r_n^{23} r_n^{34} e^{2ik_z^n h_2}}, \tag{S2}$$

where h_1 and h_2 are the thickness of the second and third layers under the vacuum layer, respectively. In consequence, r_n^{ij} is the reflectivity at the interface between layers i and j, given by the Fresnel equations

$$r_s^{ij} = \frac{k_z^{is} - k_z^{js}}{k_z^{js} + k_z^{js}}, \tag{S3}$$

$$r_p^{ij} = \frac{k_z^{ip} \varepsilon_\perp^{\,j} - k_z^{jp} \varepsilon_\perp^{\,i}}{k_z^{ip} \varepsilon_\perp^{\,j} + k_z^{jp} \varepsilon_\perp^{\,i}}, \tag{S4}$$

where

$$k_z^{is} = \left(\varepsilon_\perp^{\,i} k_0^2 - \beta^2\right)^{1/2},\ k_z^{ip} = \left(\varepsilon_\perp^{\,i} k_0^2 - \frac{\varepsilon_1^i}{\varepsilon_\parallel^{\,i}} \beta^2\right)^{1/2}.$$

When the dielectric function of each layer is known, the complex reflection coefficient of each structure unit r_n can be calculated. The reflection coefficient r_n can be further inserted into Eqs.1-2, leading to the results of the energy transmission coefficient $\xi(\omega,\beta)$ and the radiative heat flux Q.

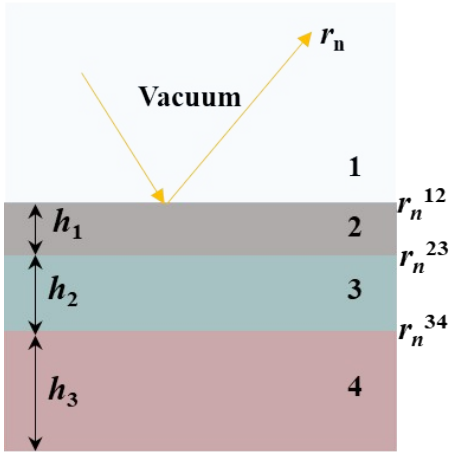

Figure S1.Schematics for detailed layers of one planar terminal heterostructure.

S2. Dielectric properties of materials used in the calculations

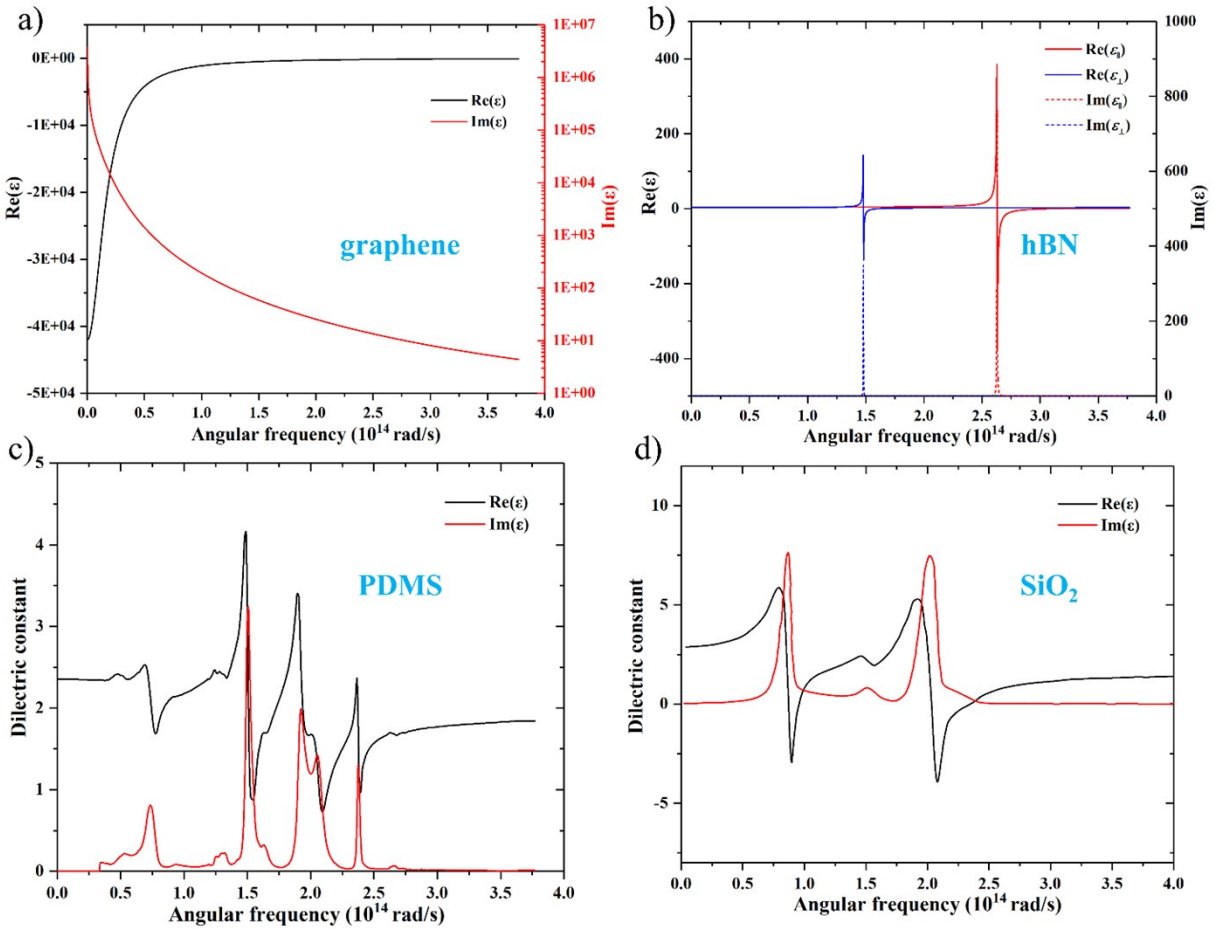

Figure S2. Dielectric constants for material used in this study: a) graphene; b) hBN; c) PDMS; d) SiO_2

S3. Comparisons of TRFs under different definitions

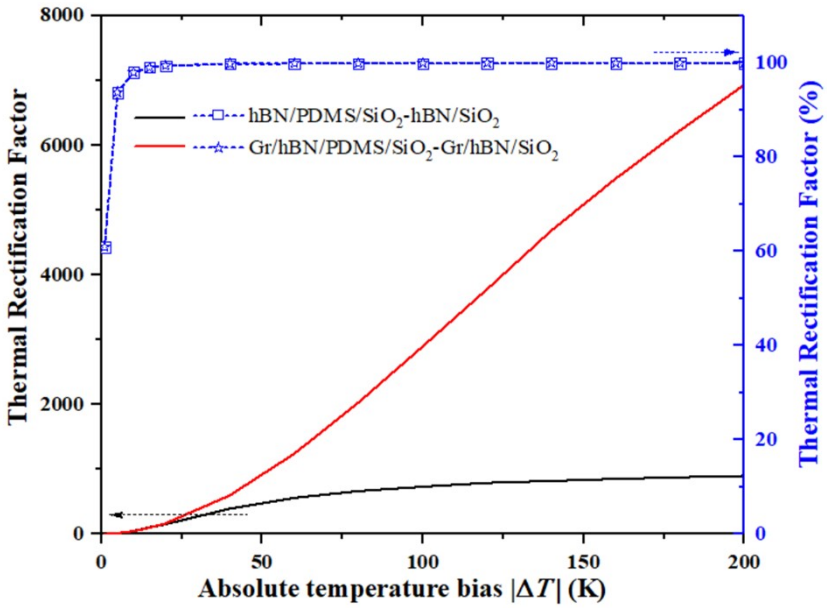

Figure S3. Comparisons of TRFs calculated under different definitions.

As for the definition of *TRF*s, both $TRF = \frac{Q_f - Q_r}{Q_r}$ (1)[4,5] and $TRF = \frac{Q_f - Q_r}{max(Q_f,\ Q_r)}$ (2)[6,7] have been used in the literature to characterize the rectification capability of NFRTRs. The latter denotes a normalized coefficient with an available range of 0~1 (i.e. 0~100%), and the extreme points of 0 and 1 respectively indicate the totally ineffective and perfect rectification capability of thermal rectifiers. We have recalculated the *TRF*s under definition (2) for cases in Fig.2a and compared them with those original values under definition (1). As illustrated in Fig.S3, the two profiles (blue dashed lines with markers) under definition (2) clearly suggest the perfect rectification capability (TRF = ~100%) of our NFRTR designs when $|\Delta T|$ is over 20 K, but these two profiles overlap so tightly that it is impossible to separate them from each other. The reason is that the range of 0~1 is too narrow to distinguish these differences, let alone the underlying mechanisms. By contrast, definition (1) has an available range of 0~∞, allowing any tiny difference plainly visible (as displayed by the red and black solid lines). Therefore, we consider that definition (1) is more appropriate to characterize the rectification capability and can serve as a powerful figure of merit for comparison between different NFRTR designs.

S4. Effects of graphene's chemical potential and hBN thickness on *TRF*s

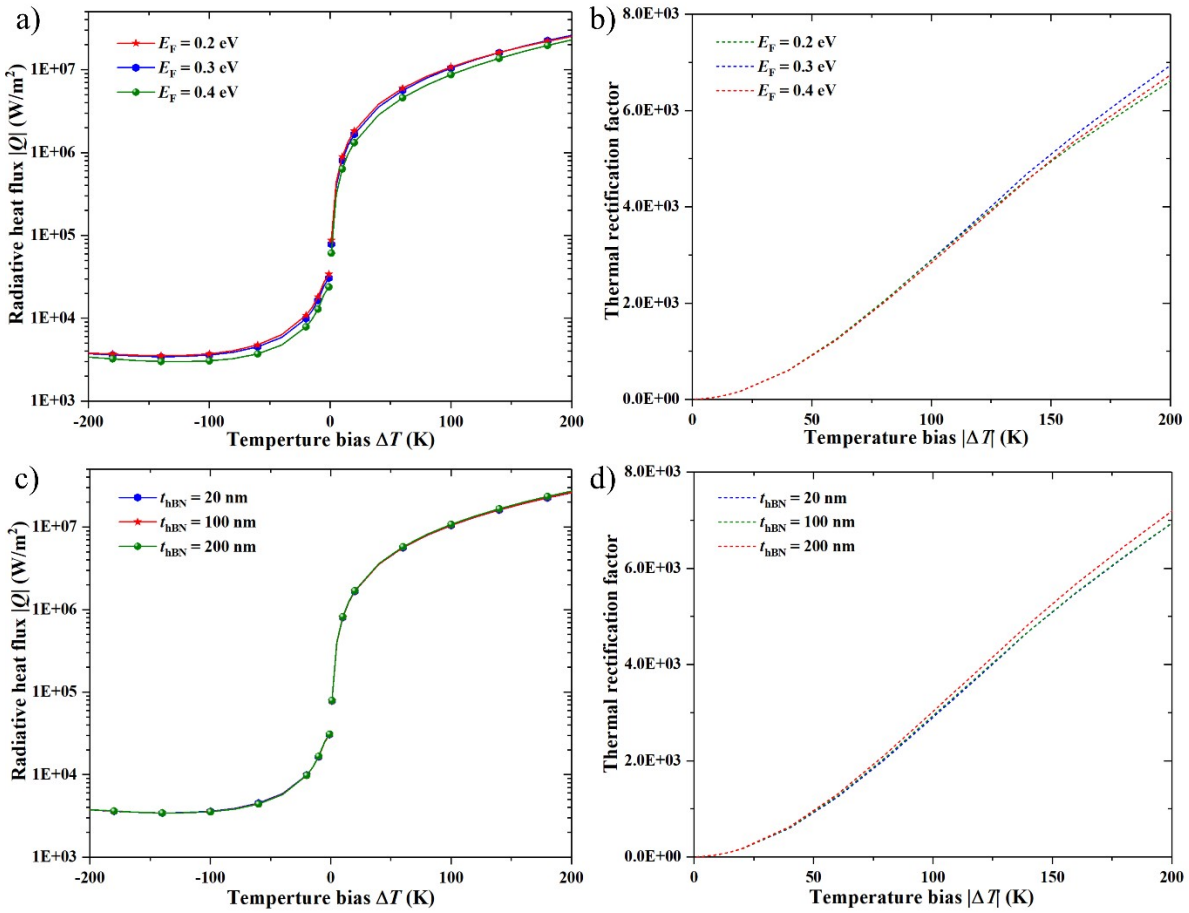

Figure S4. Thermal rectification performance of the proposed Graphene/hBN/PDMS/SiO2-Graphene/hBN/SiO2 pairings under various chemical potentials of graphene and hBN thicknesses.

Fig.S4 illustrates the effects of the chemical potential of graphene and the hBN thickness on the radiative heat flux and the resultant *TRF*s. The results show that these two parameters exert limited impacts but can be optimized to yield higher TRFs for the proposed Graphene/hBN/PDMS/SiO_2-Graphene/hBN/SiO_2 pairings. In the studied cases, pairings with a graphene chemical potential of 0.3 eV and a thicker hBN layer of 200 nm can yield higher *TRF*s (>7000).

S5. Replacing the radiative layers with other typical IR polaritonic materials

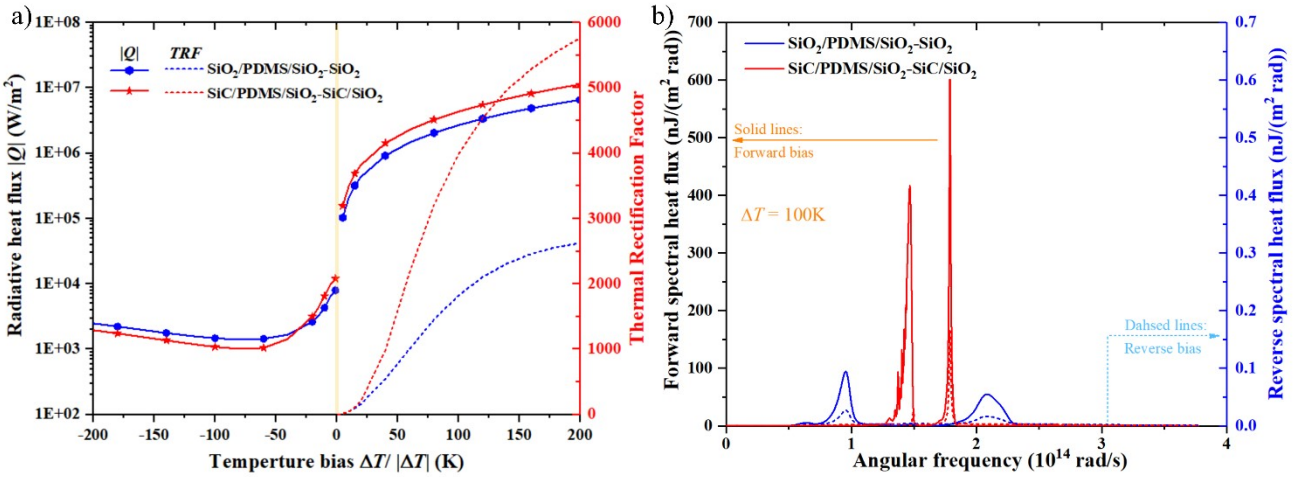

Figure S5. Thermal rectification performance of NFRTRs based on SiO_2- and SiC-involved parings. a) Radiative heat flux (solid lines with markers) and TRFs (dashed lines) as a function of temperature bias. b) Corresponding spectral heat flux under both forward and reverse bias at $\Delta T = 100$ K.

The radiative layers can be replaced by other materials supporting IR polaritons, such as SiO_2 and SiC most commonly adopted in nanophotonics. As displayed in Fig.S5a), high TRFs have also been achieved as ~2620 and ~5760 for SiO_2/PDMS/SiO_2-SiO_2 and SiC/PDMS/SiO_2-SiC/SiO_2 parings, respectively. The profiles of spectral heat flux in Fig.S5b) show little difference in the peak positions but high contrasts in amplitudes. These peaks highlight the contribution of surface phonon polaritons to the heat flux while the dramatic drop in the amplitudes of heat flux originates from the exponentially decaying of these evanescent modes with increasing gap sizes. These results further indicate the design flexibility of the proposed design scheme for highly-efficient NFRTRs.

S6. Comparisons of TRFs with previous reports

Table S1. Comparisons of TRFs achieved for NFRTRs in previous publications and the present work

Refs	Terminal material pairings	$\lvert\Delta T\rvert$ (K)	Gap size (nm)	TRFs
Otey et al.[5]	SiC-3C to SiC-6H	300	100	0.41
Basu et al.[8]	doped Si to doped Si	100	10	0.5
Wang et al.[4]	intrinsic Si to SiO_2	700	10	2.55
Feng et al.[9]	hBN to InSb	200	10	17
Yang et al.[10]	VO_2 to SiO_2	100	20	2
Zheng et al.[11]	Gra*/VO_2 to SiO_2	53	10	3.8
Li et al.[12]	VO_2 to cBN	20	100	140
Li et al.[13]	VO_2 nanowires to cBN nanowires	20	100	324
Liu et al.[14]	VO_2 grating/KBr to cBN/Au	20	100	161
This work	hBN/PDMS/SiO_2 to hBN/SiO_2	20	d_f=10; d_r=1000	9597
This work	Gra/hBN/PDMS/SiO_2 to Gra/hBN/SiO_2	20	d_f=10; d_r=1000	9980

*In this table, Gra is short for graphene.

S7. Detailed fitting parameters for $Q = \gamma d^n$

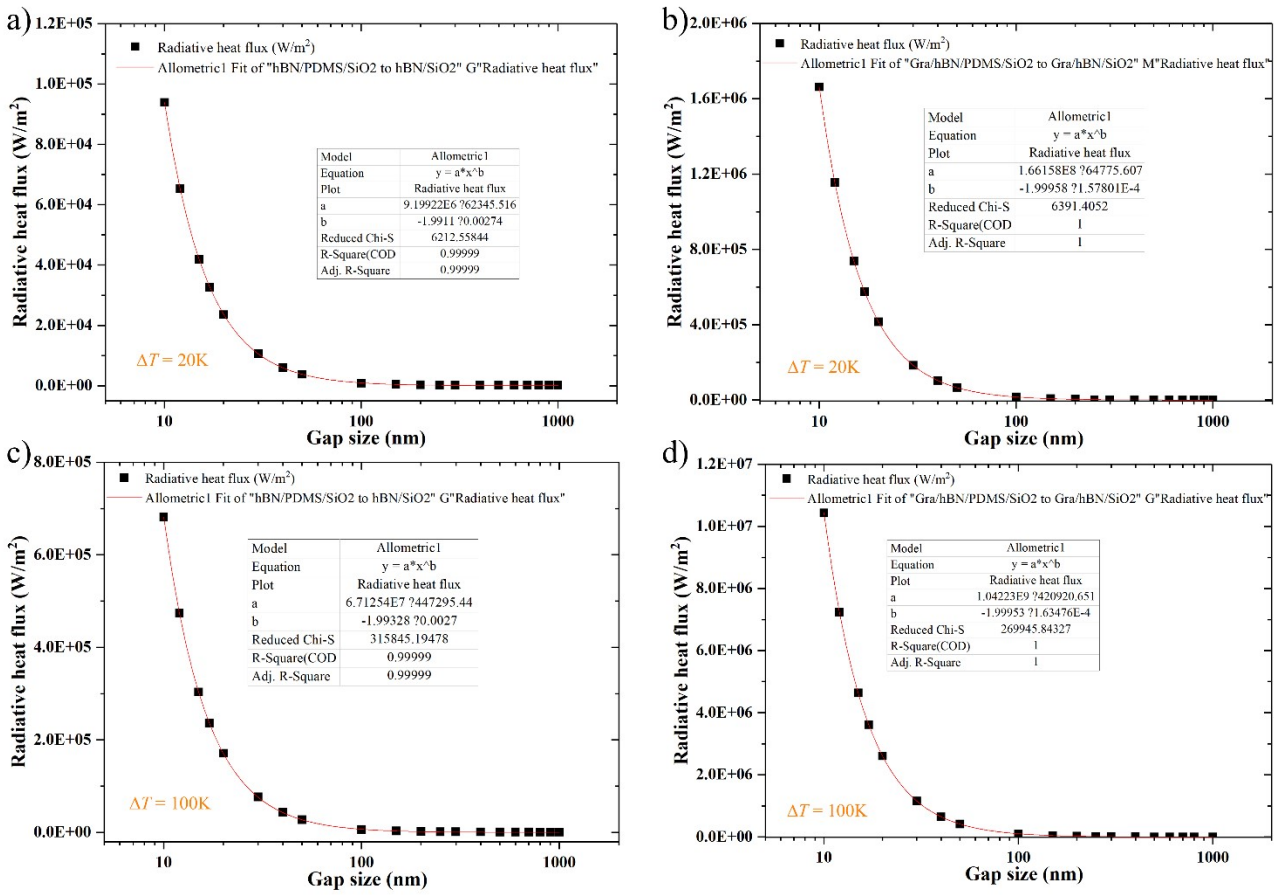

Figure S6. Detailed fitting parameters for gap-size-dependence of the radiative heat flux for both hBN- and graphene/hBN-based pairings under different temperature gradients: a, b) 20 K and c, d) 100 K.

References

1 S. Dai, Z. Fei, Q. Ma, A. S. Rodin, M. Wagner, A. S. McLeod, M. K. Liu, W. Gannett, W. Regan, K. Watanabe, T. Taniguchi, M. Thiemens, G. Dominguez, A. H. Castro Neto, A. Zettl, F. Keilmann, P. Jarillo-Herrero, M. M. Fogler and D. N. Basov, *Science (80-.).*, 2014, **343**, 1125–1129.

2 B. Song, Y. Ganjeh, S. Sadat, D. Thompson, A. Fiorino, V. Fernández-Hurtado, J. Feist, F. J. Garcia-Vidal, J. C. Cuevas, P. Reddy and E. Meyhofer, *Nat. Nanotechnol.*, 2015, **10**, 253–258.

3 B. Yang, D. Pan, X. Guo, H. Hu and Q. Dai, *Int. J. Therm. Sci.*, 2022, **176**, 107493.

4 L. P. Wang and Z. M. Zhang, *Nanoscale Microscale Thermophys. Eng.*, 2013, **17**, 337–348.

5 C. R. Otey, W. T. Lau and S. Fan, *Phys. Rev. Lett.*, 2010, **104**, 1–4.

6 A. Fiorino, D. Thompson, L. Zhu, R. Mittapally, S. A. Biehs, O. Bezencenet, N. El-Bondry, S. Bansropun, P. Ben-Abdallah, E. Meyhofer and P. Reddy, *ACS Nano*, 2018, **12**, 5174–5179.

7 I. Latella, P. Ben-Abdallah and M. Nikbakht, *Phys. Rev. B*, 2021, **104**, 1–8.

8 S. Basu and M. Francoeur, *Appl. Phys. Lett.*, 2011, **98**, 1–4.

9 D. Feng, S. K. Yee and Z. M. Zhang, *Appl. Phys. Lett.*, 2021, **119**, 181111.

10 Y. Yang, S. Basu and L. Wang, *Appl. Phys. Lett.*, 2013, **103**, 163101.

11 Z. Zheng, X. Liu, A. Wang and Y. Xuan, *Int. J. Heat Mass Transf.*, 2017, **109**, 63–72.

12 Q. Li, H. He, Q. Chen and B. Song, *Phys. Rev. Appl.*, 2021, **16**, 014069.

13 Q. Li, H. He, Q. Chen and B. Song, *Phys. Rev. Appl.*, 2021, **16**, 064022.

14 Y. Liu, Y. Tian, F. Chen, A. Caratenuto, X. Liu, M. Antezza and Y. Zheng, *Appl. Phys. Lett.*, 2021, **119**, 123101.